International Journal of Power and Energy Systems, Vol. 44, No. 10, 2024
An Open Access Paper

INFLUENCE OF POLES ON PERFORMANCE OF AN ELECTRICAL MACHINE

Chukwuemeka Chijioke Awah*

Abstract

Influence of rotor pole number on electromagnetic performance of an electrical machine is examined in this study. The investigated machine is a double stator flux-switching permanent magnet machine (DSFSPM). The study is carried out with the aid of Maxwell-2D finite element software. The predicted variables are: flux linkage, electromotive force (EMF), demagnetisation capability, power, and torque. The compared different rotor topologies are: $N_r = 10$, $N_r = 11$, $N_r = 13$, and $N_r = 14$, where Nr represents the number of rotor poles. The analysis shows that the most optimum combination of the different investigated topologies, capable of producing the largest torque and EMF magnitudes is the 6 stator slot/11 rotor pole combination, *i.e.*, the machine topology that has $N_s = 6$ and $N_r = 11$, where N_s and N_r is the stator slot number and rotor pole number, respectively. However, the machine topology that has $N_r = 10$, would produce the least amount of torque and EMF values. Also, the machine topology having $N_r = 14$ would generate the least value of flux linkage per phase, likely due to the influence of its enormous harmonic elements. The predicted fundamental EMF amplitude of the compared different topologies having $N_r = 10$, $N_r = 11$, $N_r = 13$, and $N_r = 14$ is 2.64 V, 5.28 V, 5.01 V, and 3.15 V, respectively. The resulting fundamental electromagnetic torque value of the compared different topologies, obtained using fast Fourier transform (FFT) technique is 1.39 Nm, 2.78 Nm, 2.63 Nm, and 1.66 Nm, respectively. The compared different topologies exhibit high tendency to withstand demagnetisation effect, both at high load and high speed conditions. The investigated machine would be ideal for direct-drive operations, due to its low-speed high-torque potentials.

Key Words

High-torque, low-speed, machine, pole combinations, rotor and stator

1. Introduction

The feasible combinations of stator slot and rotor pole numbers of electrical machines have been researched; however, more research is still ongoing in this regard, due the huge impact these pole numbers could have on the machine's performance. Thus, the influence of rotor poles of a given double stator permanent magnet (PM) machine is explored in this investigation, to determine the most optimal rotor pole number for a good output performance. The investigated machine in this current study is a typical flux-switching permanent magnet machine (FSPM); though, it has double stator structure and different rotor pole numbers. The machine's pole ratio, which customarily depends on rotor pole number of the machine, plays a significant role in its output performance, as demonstrated in [1] and [2]; and this would invariably influence the machine's winding factor [3]. The reason is because, the winding terminal connections/polarities and the operating speed of a given PM machine is dependent on its pole number, as highlighted in [4]. The dependency of a machine's winding factor on the number of rotor poles is re-emphasised in [5].

Also, it is established in [6] that the stator slot and rotor pole numbers of a given electrical machine, as well as the machine's optimal structural parameters are very essential in determining its resulting output performance(s) and characteristics. It is also noted that adequate machine design of a model achieved through implementation of these slot number and pole number parameters, would yield the most economical product, in addition to an improved electromagnetic output. Similarly, control amenability and the mechanical stability of a given electrical machine could be influenced by its stator slot and rotor pole permutations, as could be deduced from [7], besides its usual effects on the machine's electromagnetic output performances.

Further, the torque production and transmission of Vernier PM machine which works on the principle of magnetic gearing of the modulated magnetic fields would also depend upon the following parameters: number of slots, number of magnet pole pairs and winding pole pairs, as stated in [8]. It is worth noting that the magnet pole pairs of such machines are related to its number of rotor poles. Meanwhile, it is stated that FSPMs that have high rotor pole number, would consequently exhibit higher flux leakages [9]. However, the flux leakage from a given electric machine could be minimised by adopting a Halbach magnetisation technique for enhanced air gap flux density, as presented in [10]; flux-leakage reduction

* Department of Electrical and Electronic Engineering, Michael Okpara University of Agriculture, Umudike, Nigeria; e-mail: awahchukwuemeka@gmail.com
Corresponding author: Chukwuemeka Chijioke Awah

(DOI: 10.2316/J.2024.203-0480)

could also be achieved by implementing a consequent PM-pole technique, as noted in [8]. All the same, the number of stator slots of electric machines would affect the resulting values of the machine's electromagnetic performance considerably, as revealed in [11]; however, the analyses in this current study are limited to the influence of rotor pole numbers on the machine's output performance.

Traditional fractional-slot concentrated-wound permanent magnet synchronous machine (FSCW-PMSM) customarily has little no-load torque and enhanced fault tolerance potential, compared to most PM machines, as noted in [12]. However, the investigated FSPM machine in this current study naturally has good thermal management feature and hence; superior capability to withstand demagnetisation effects, compared to other PM machines like the FSCW-PMSM, owing to its suitably stator-mounted magnet arrangement. Nevertheless, FSPM machines exhibit two exclusive characteristics compared to other PM machines [13]: (a) Adjacent stator cores must have opposite magnetisation paths (b) Intrinsic ability to possess odd number of poles. Mores so, FSPM machines essentially have sinusoidal electromotive force (EMF) waveforms, as established in [14]. However, the generated EMF value of a typical FSPM machine is inversely related to the order of its flux density harmonics; the lesser these harmonic orders, then, the larger its resulting EMF amplitude and *vice-versa*. It is important to note that FSPM machines generally have two torque components, namely: the PM torque component and reluctance torque component, basically due to magnet and armature winding excitations.

Further, the study in [15] revealed that torque capability and field-weakening potential of a given PM machine would be greatly influenced by the relative difference between the machine's rotor pole and stator slot numbers.

Basically, the influence of rotor poles of a given double stator electrical machine is studied in this present investigation; to estimate the impact of these poles on machine's output performance. The investigated machine can produce reasonable electromagnetic at low speed, and this feature is desirable in direct-drive machine applications. The organisation of this study is thus: First, background of study as well as the reviewed literature are introduced and provided in Section 1. The adopted materials and method are presented in Section 2. The predicted results are compared and discussed in Section 3. The analyses are concluded in Section 4.

2. Materials and Method

The results in this work are obtained through finite element analysis (FEA), by applying MAXWELL-2D software. The coil electromotive force (E_c) of a given FSPM is predicted using (1). Also, the electromagnetic torque (T) of the analysed machine is estimated using (2). The rotor and stator cores are made of steel material while the PMs are of rare-earth class, *i.e.*, N35SH. On exciting the armature windings by a three-phase alternating current,

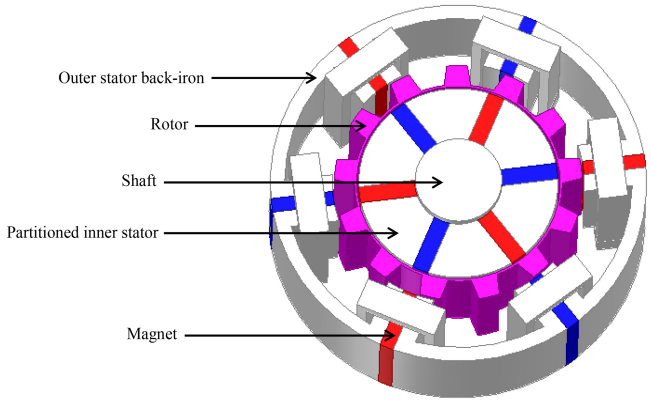

Figure 1. The analysed machine structure [20].

EMF would be induced in the coils and the induced EMF would cause the rotating modulating ring, *i.e.*, the rotor to start rotating. Eventually, an electromagnetic torque is produced in the system through an electromagnetic energy conversion process at the machine's air gap region. It is worth mentioning that the analysed machine would function as both flux-switching and magnetically-geared machine, owing to its inherent dual operating characteristics. Meanwhile, the implemented stator slot number (N_s) and rotor pole number (N_r) in this current study are mathematically expressed in (3) and (4), as deduced from [16]. The analysed machine model having thirteen (13) rotor poles is displayed in Fig. 1. It is important to note that the investigated machine in this current study is a double stator flux-switching permanent magnet machine (DSFSPM). Double stator permanent machines naturally have larger output torque compared to its single stator counterparts, as confirmed in [17]; nevertheless at higher cost penalty. The basic parameters of the analysed machine topologies are given in Table 1.

$$E_c = -\frac{\mathrm{d}\psi}{\mathrm{dt}} = -\frac{d}{\mathrm{dt}} \int_{\theta}^{\frac{N_r}{N_s}\pi+\theta} N_c R_{\mathrm{out}} L_a B(\theta)\, \mathrm{d}\theta \qquad (1)$$

where: ψ is the flux linkage per phase, N_r and N_s are the rotor pole number and stator slot numbers, N_c is the number of turns per coil, $B(\theta)$ is the flux density at a given rotor position, R_{out} is the stator outer radius, and L_a is the effective length of the machine [9].

$$T = 1.5N_r \left(\lambda_m I_q + (L_d - L_q)\, I_d I_q\right) \qquad (2)$$

where: N_r is the rotor pole number, λ_m is the magnet flux linkage, I_q is the quadrature axis current, I_d is the direct-axis current, and L_q and L_d are the axes inductances [18].

The rotor pole number of an FSPM machine corresponds to number of rotor pole pairs of a traditional PM machine [19]. The ability to exhibit both even and odd number of rotor poles is a peculiar property that is unique to FSPM machines, compared to other conventional machines [13].

$$N_r = 2N_s \pm 1 \qquad (3)$$

$$N_r = 2N_s \pm 2 \qquad (4)$$

Table 1
Basic Machine Parameters

Machine parameter	Values			
Pole number (Nr)	10	11	13	14
Rotor weight, kg	0.0214	0.0281	0.0238	0.0214
Outer rotor radius, mm	31.25	32.63	29.64	31.25
Stator slot number	6			
Number of permanent magnet poles per stator	6			
Outer stator radius, mm	45			
Magnet permeability	1.05			
Operating speed, r/min	400			
Rated current, A	15			
Employed magnet type	N35SH			
Stator and rotor core material	M330-35A			
Coil resistivity	1.68e-008			
Operating temperature, ^{o}C	20			
Magnetic remanence, T	1.2			
Packing factor	0.6			
Number of turns per phase	72			

The field-weakening potential (k_f) of a given PM machine is predicted with (5).

$$k_f = \frac{L_d I_m}{\psi_{\mathrm{pm}}} \tag{5}$$

Where: I_m is the supplied peak current and ψ_{pm} is the PM flux linkage [21].

3. Results and Discussion

Figure 2 shows the magnetic flux line distributions of the compared different topologies. The generated flux per pole is seen to be more concentrated when $N_r = 11$. Similarly, the flux linkage waveforms of the compared topologies are presented in Fig. 3. It is shown that the machine topology having $N_r = 11$ has the largest amount of magnetic flux linkage per phase. The largest and least fundamental flux linkage amplitude of the different topologies is obtained when $N_r = 11$ and $N_r = 14$, respectively. This is obtained using the fast Fourier transform (FFT) technique. More so, the noticeable second (2^{nd}) order spectrum of Fig. 3(b) shows that the analysed machine topology having $N_r = 10$ and $N_r = 14$, would suffer from harmonic issues; particularly, during control operations. Also, the EMF waveforms of the different topologies are depicted in Fig. 4. It is worth noting that the generated EMF of any machine would be dependent upon the changing rate of its flux with time. The $N_r = 10$ and $N_r = 14$ machine topologies are adversely affected by their high harmonic contents, over time. This is obviously shown in the more asymmetric and non-sinusoidal nature of the EMF waveforms, compared to its corresponding flux linkage waveforms. More so, the studies in [22] and [23] revealed that a given electrical machine that produces higher flux linkage value may not necessarily generate higher value of EMF and corresponding torque magnitudes. This concept of flux linkage value and its consequent output performances is in-line with the predicted results presented in [7].

Again, the presence of even order harmonic spectra in Fig. 4(b) shows that the machine model having $N_r = 10$ and $N_r = 14$ would not be reasonably agreeable to electric machine control operation(s). Moreover, since the compared topologies have little amount of seventh (7^{th}) order EMF harmonics; then, the different topologies would have low amount of torque ripple, as suggested in [22]. Therefore, the larger the value of the seventh (7^{th}) EMF harmonic order in electric machines, then, the lesser the resulting average torque in such electric device and *vice-versa*. The peak value of EMF in the compared machines is: 3.07 V, 5.36 V, 4.99 V, and 2.91 V, *i.e.*, from the $N_r = 10$, $N_r = 11$, $N_r = 13$, and $N_r = 14$ models, respectively. More so, it is shown in Fig. 4(c) that there is a linear relationship between the generated voltage of a given electric machine and its applied electromagnetic loads; thus, the higher the applied load, then, the larger the resulting voltage and *vice-versa*. It is also worth noting that the resultant

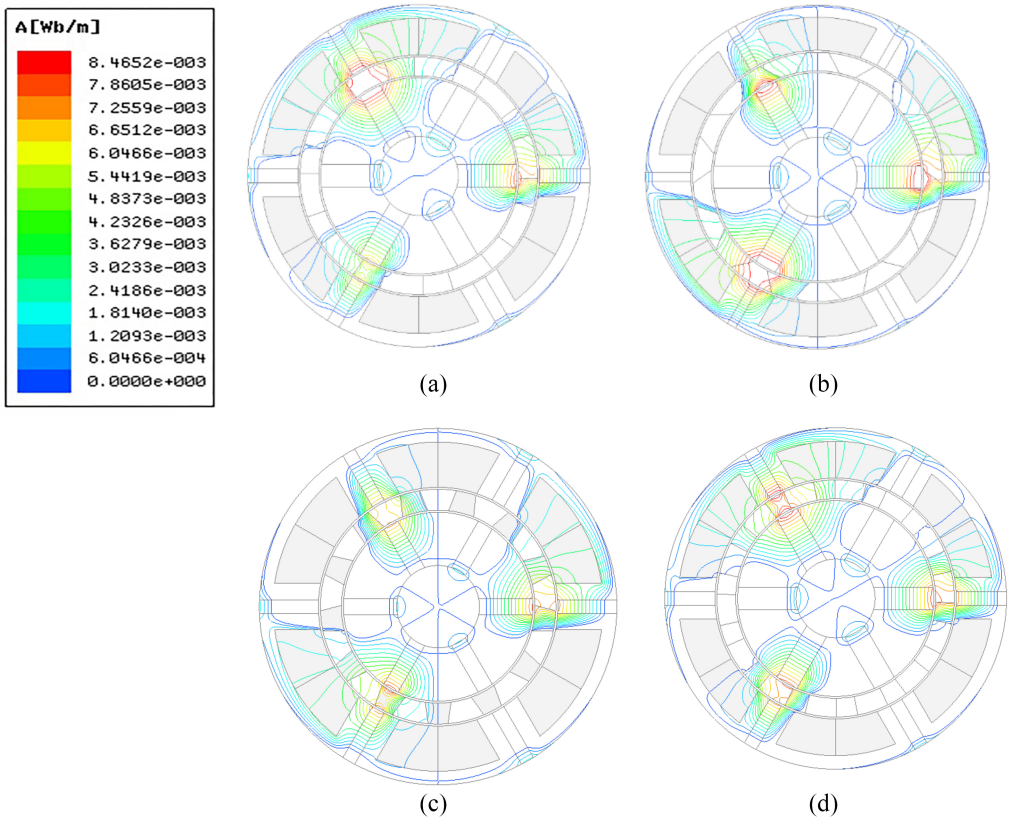

Figure 2. Flux line contours: (a) $N_r = 10$; (b) $N_r = 11$; (c) $N_r = 13$; and (d) $N_r = 14$.

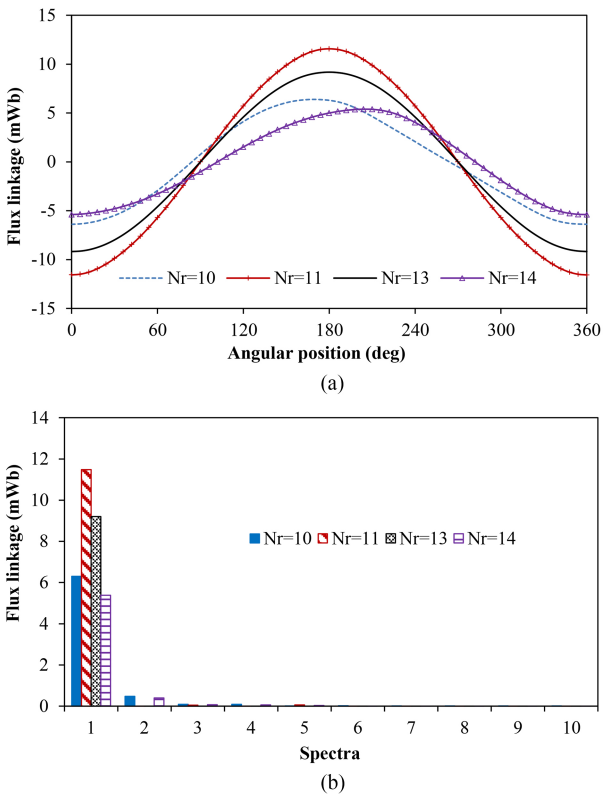

Figure 3. Flux linkage comparisons at 400 r/min: (a) flux linkage versus angular position and (b) flux linkage FFT.

voltage amplitude in such system would depend upon the value of the applied load, as well as on the natural effect of electromagnetic saturation of the conductors and the magnets.

Figure 5 (a) depicts the electromagnetic torque waveforms of the compared machine models, simulated at rated current of 15 A with rotational speed of 400 r/min. The obtained peak value of electromagnetic torque from the $N_r = 10$, $N_r = 11$, $N_r = 13$, and $N_r = 14$ models is 2.72 Nm, 2.92 Nm, 2.77 Nm, and 2.19 Nm, respectively. The least performing machine model is the one having $N_r = 10$. Meanwhile, the presence of sixth (6^{th}) harmonic torque component shown in Fig. 5(b) suggests that compared topologies are not free of both cogging torque and torque pulsation components. Moreover, the manifestation of third (3^{rd}) order harmonic component in Fig. 5(b) indicates that the analysed machine topologies having $N_r = 10$ and $N_r = 14$ would have relatively high amount of torque ripple, as inferred from [24].

Further, the variation of average torque with supplied peak current is compared in Fig. 6(a). It is observed that the largest amount of torque is achieved when $N_r = 11$, this is followed by the result of $N_r = 13$, over the entire simulation loading conditions. Note that the machine model that has $N_r = 10$, exhibits the least amount of average torque. Note also that the withstand ability of the compared topologies against electric overload or armature saturation effect is denoted by its resulting value in Fig. 6(a). More so, the variation of torque per magnet

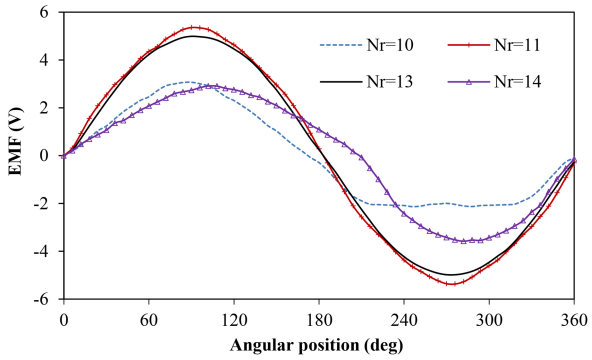

(a)

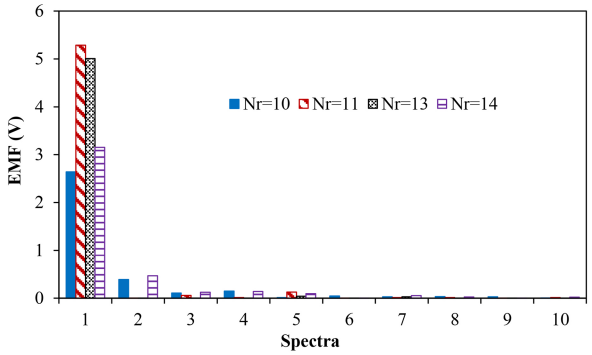

(b)

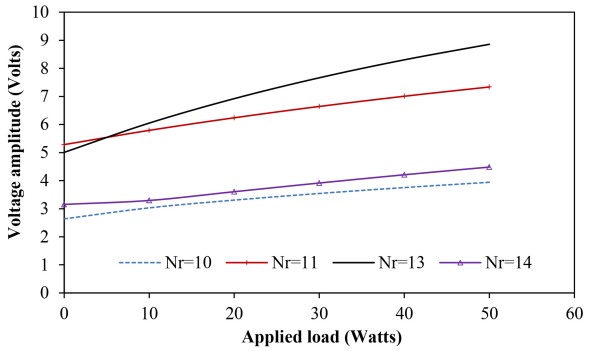

(c)

Figure 4. The compared phase EMF at 400 r/min: (a) EMF versus angular position; (b) EMF FFT; and (c) induced voltage amplitude versus applied load.

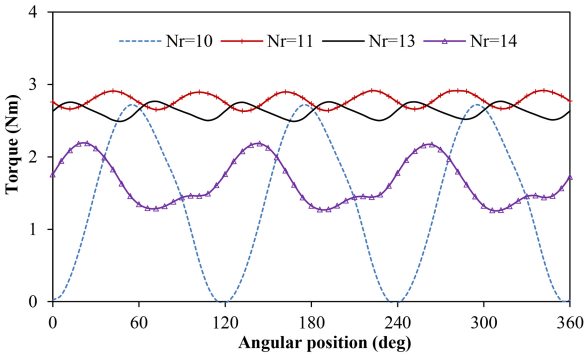

(a)

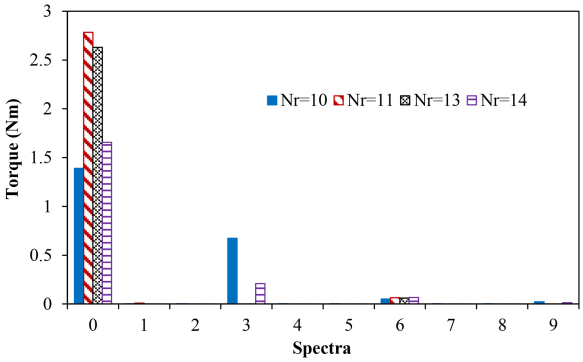

(b)

Figure 5. Torque comparisons at 15 A, 400 r/min: (a) torque versus angular position and (b) torque FFT components.

usage shown in Fig. 6(b) reveal that the machine having $N_r = 11$ is the best candidate at all the loading conditions; this is followed by its counterpart having $N_r = 13$. It could be deduced from Fig. 6(b), that the $N_r = 11$ model would be the cheapest to construct in practice, bearing in mind its output performance in relation to the employed magnet material and or volume.

The power–speed and torque–speed envelopes of the compared machine topologies are displayed in Fig. 7(a) and 7(b), respectively. The maximum power obtained in the machine is 498.61 W, 498.56 W, 498.52 W, and 498.54 W, *i.e.*, from the $N_r = 10$, $N_r = 11$, $N_r = 13$, and $N_r = 14$ machine topologies. Hence, the compared topologies have fairly similar amount of maximum output power. Similarly, the resulting output torque from the topologies, from the constant torque region is 1.40 Nm, 2.78 Nm, 2.63 Nm, and 1.69 Nm, respectively. It is observed that the machine configuration having $N_r = 13$ and $N_r = 14$ would have higher potential to operate over a wider speed range; and this wide-speed coverage is a desired quality in field-weakening operations of electric machines, for traction and automobile applications. It is worth mentioning that the capability of a machine to operate over a wide-speed range is dependent upon the machine's direct-axis inductance, applied current and its PM flux value, as implied in [21] and [25]. More so, a particular machine configuration that produces the largest amount of torque may not essentially have superior speed range, as established in [25] and [26]. The assertion about higher output torque of an electrical machine over narrower speed coverage is reconfirmed in [27]. Note that the ability of the machine to operate over a wider speed range is an indication of the machine's field-weakening potential. Moreover, the compared machine categories are initially optimised using the inherent genetic algorithm of the employed MAXWELL-2D software at constant copper loss condition, for maximum average torque, without considering the machine's optimal power and load angle, and also without prejudice to the machine's back-EMF and base speed, as detailed in [28]. It is worth noting that the applied current and voltage are constrained to its maximum limits, I_m and V_m, respectively. Further, field-weakening capability of a given machine is directly related to the ratio of the machine's maximum speed to base speed (R_N), as noted in [29]. The field-weakening potential (k_f) of the compared machine topologies is listed

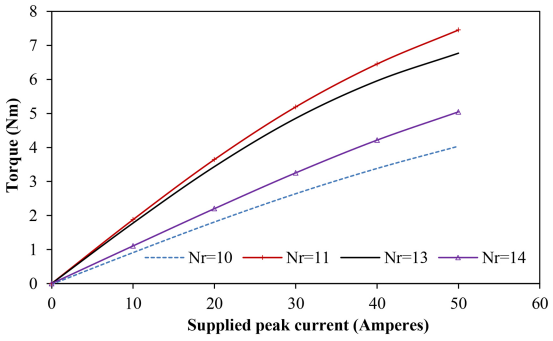

(a)

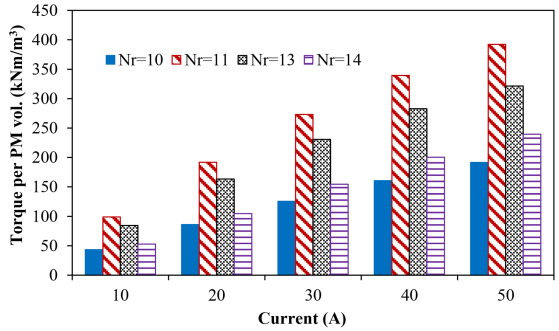

(b)

Figure 6. Comparison of torque per magnet volume at 400 r/min: (a) torque versus supplied current and (b) torque per magnet volume.

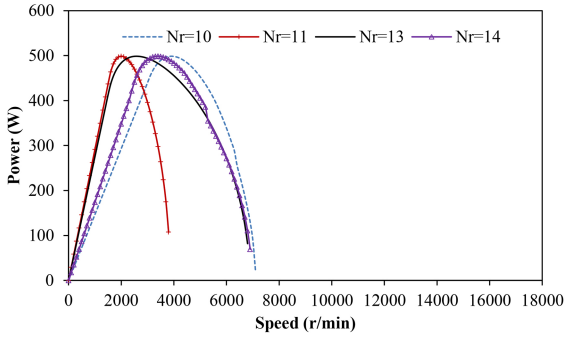

(a)

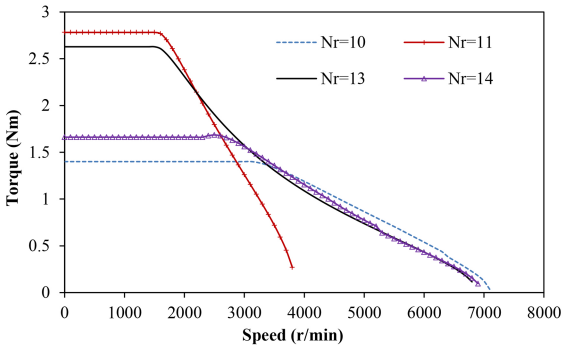

(b)

Figure 7. Torque and power speed characteristics at 15 A, 22.9 V: (a) power versus speed and (b) torque versus speed.

in Table 2. A higher value of this speed ratio (R_N) or and k_f would imply a better constant power machine operation, *i.e.*, in the extended speed range/region; and

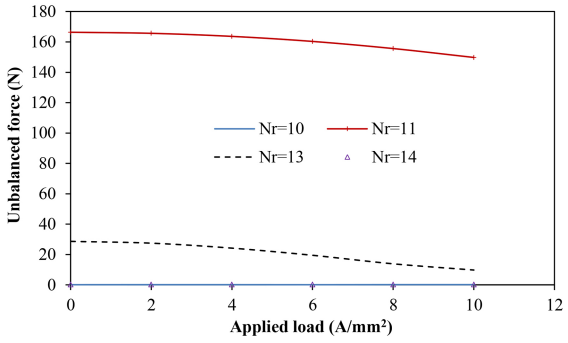

(a)

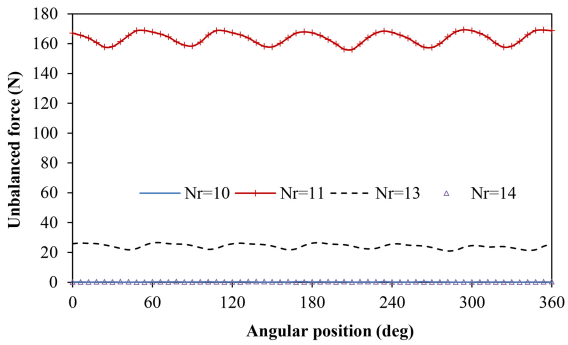

(b)

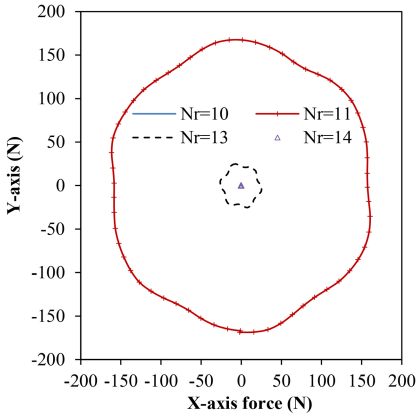

(c)

Figure 8. Comparison of unbalanced magnetic force: (a) force versus current density; (b) force versus rotor angular position, at 4 A/mm^2; and (c) force magnitude in X- and Y-axis, at 4 A/mm^2.

thus, a signal of the machine's greater field-weakening ability.

Furthermore, the magnitudes of unbalanced magnetic force (UMF) on the rotor of compared machine topologies are presented in Fig. 8. It is shown that the machine topology having $N_r = 2N_s \pm 1$ would have larger amount of UMF on the rotor compared to the ones that have $N_r = 2N_s \pm 2$; the resulting magnetic force amplitude from the latter category of machine is relatively negligible to that of the former. It can also be deduced that applied electric load could influence the amplitude of these forces, especially when the machine is overloaded. It is evident from Fig. 8(b) that the magnitude of these UMF would be slightly dependent upon the machine's rotor

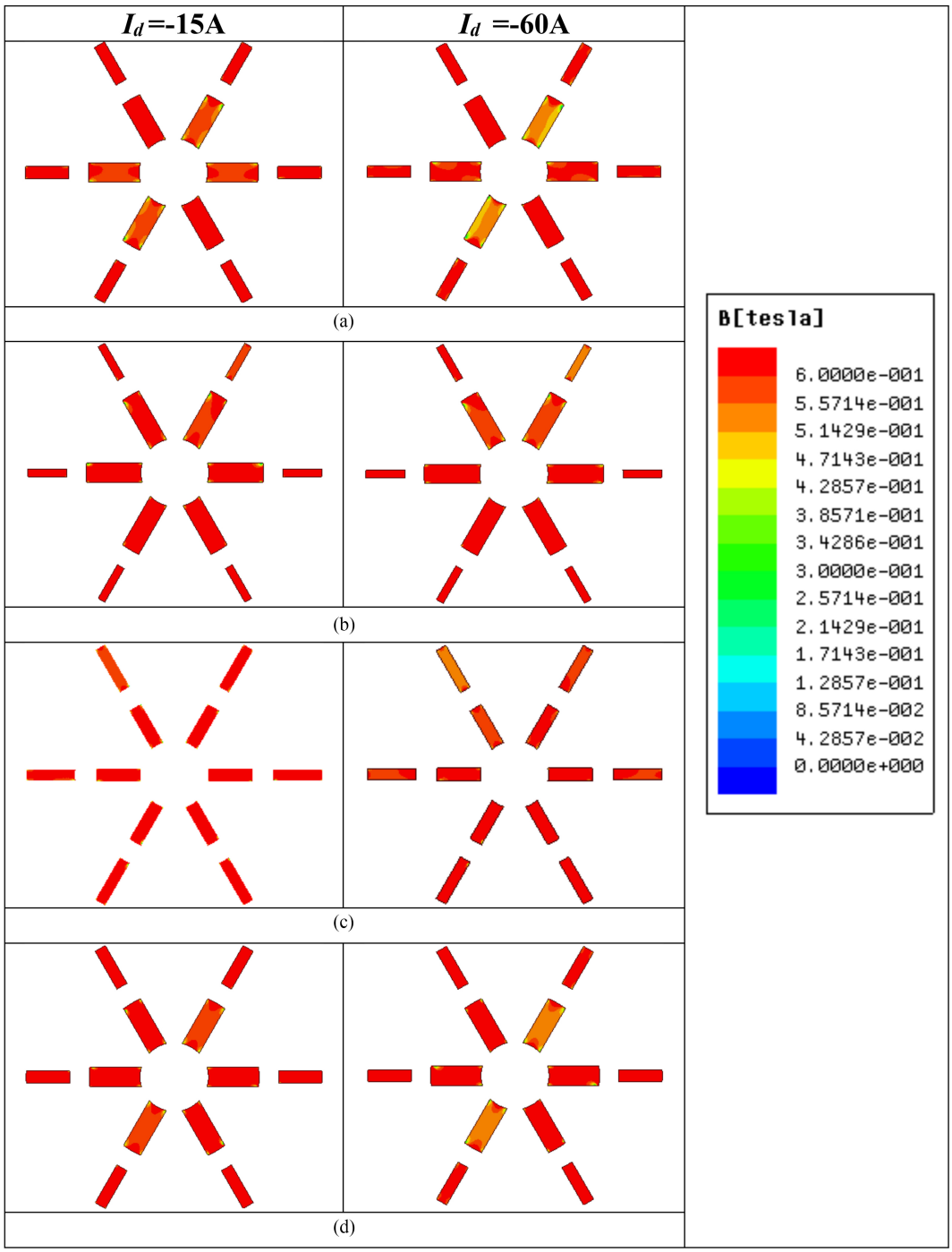

Figure 9. Demagnetisation distributions of the compared topologies at 4,000 r/min and 20°C: (a) $N_r = 10$; (b) $N_r = 11$; (c) $N_r = 13$; and (d) $N_r = 14$.

angular positions. Although, the machine topology that have $N_r = 11$ and $N_r = 13$ exhibit larger UMF, owing to the nature of its pole number; its output torque is larger than that of $N_r = 10$ and $N_r = 14$ machine topologies. Nevertheless, high amount of UMF can cause vibration and noise in a machine [16]. Electrical machines that are equipped with odd number of rotor poles would naturally have high level of UMF, as proved in [7] and [30].

Figure 9 shows the FEA predicted demagnetisation contours/distributions of the different topologies. It is observed that the compared topologies would be able to withstand demagnetisation influence, even at high field-weakening operation state. It is also noticed that areas of the topologies that may easily be susceptible to demagnetisation influence, possibly during heavy electromagnetic overload and saturation conditions are quite different and specific for each machine topology. Generally, FSPMs exhibit good anti-demagnetisation skills; though, the temperature effect and thermal stability of a given permanent machine would greatly affect the capability of such machine to withstand demagnetisation impact, as discussed in [10] and [31]. More so, it is deduced

Table 2
Field-Weakening Potential

Item	Value			
Pole number	Nr = 10	Nr = 11	Nr = 13	Nr = 14
Maximum speed ($N_{\max}$), r/min	7,100	3,800	6,800	6,900
Base speed (N_{base}), r/min	3,000	1,500	1,500	2,300
Ratio of $N_{\max}$:N_{base} (R_N)	2.37	2.53	4.53	3.00
Supplied maximum current (I_m), A	15			
Direct axis inductance (L_d), mH	0.204	0.371	0.404	0.189
Field-weakening potential (k_f)	0.4951	0.4955	0.6748	0.5462
Permanent magnet flux (ψ_{magnet}), mWb	6.18	11.23	8.98	5.19

from [32] that by deploying suitable structural architecture of a given PM machine, its undesirable elements, such as voltage harmonics and demagnetisation vulnerabilities could be greatly reduced.

4. Conclusion

The influence of rotor poles of an electrical machine is studied and compared amongst four different machine rotor topologies. The compared machine topology having $N_r = 11$ yields good performance qualities, such as: highest flux linkage and EMF values, largest amount of electromagnetic and average torque, more symmetrical and sinusoidal EMF waveforms. These good performance qualities are necessary for efficient control of electrical machines. However, the machine topology that has $N_r = 13$ exhibits the best field-weakening potential, owing to its admirable field-weakening factor, as well as its high maximum speed to base speed ratio. This is followed by that of $N_r = 14$ machine topology. The compared different topologies have almost similar peak output power at the rated current and speed conditions. Moreover, the compared different topologies have impressive anti-demagnetisation capabilities even at field-weakening operating modes. The relevance of the compared topologies is dependent upon its specific application(s).

Statements and Declarations

No funding was received for conducting this study and the authors have no conflict of interest(s) to declare.

References

[1] L. Wu, R. Qu, D. Li, and Y. Gao, Influence of pole ratio and winding pole numbers on performance and optimal design parameters of surface permanent-magnet Vernier machines, *IEEE Transactions on Industry Applications*, *51*(5), 2015, 3707–3715.

[2] Y. Gao, R. Qu, D. Li, J. Li, and G. Zhou, Design of a dual-Stator LTS vernier machine for direct-drive wind power generation, *IEEE Transactions on Applied Superconductivity*, *26*(4), 2016, 1–5.

[3] W. Hua, H. Zhang, M. Cheng, J. Meng, and C. Hou, An outer-rotor flux-switching permanent-magnet-machine with wedge-shaped magnets for in-wheel light traction, *IEEE Transactions on Industrial Electronics*, *64*(1), 2017, 69–80.

[4] Y. Shi, L. Jian, J. Wei, Z. Shao, W. Li, and C.C. Chan, A new perspective on the operating principle of flux-switching permanent-magnet machines, *IEEE Transactions on Industrial Electronics*, *63*(3), 2016, 1425–1437.

[5] W. Liu and T.A. Lipo, Analysis of consequent pole spoke type vernier permanent magnet machine with alternating flux barrier design, *IEEE Transactions on Industry Applications*, *54*(6), 2018, 5918–5929.

[6] D. Li, R. Qu, J. Li, and W. Xu, Consequent-pole toroidal-winding outer-rotor Vernier permanent-magnet machines, *IEEE Transactions on Industry Applications*, *51*(6), 2015, 4470–4481.

[7] M. Zheng, Z.Q. Zhu, S. Cai, H.Y. Li, and Y. Liu, Influence of stator and rotor pole number combinations on the electromagnetic performance of stator slot-opening PM hybrid-excited machine, *IEEE Transactions on Magnetics*, *55*(5), 2019, 1–10.

[8] H. Gorginpour, Design modifications for improving modulation flux capability of consequent-pole vernier-PM machine in comparison to conventional vernier-PM machines, *Scientia Iranica D*, *27*(6), 2020, 3150–3161.

[9] H. Zhang, W. Hua, and G. Zhang, Analysis of back-EMF waveform of a novel outer-rotor-permanent-magnet flux switching machine, *IEEE Transactions on magnetics*, *53*(6), 2017, 1–4.

[10] M. Kang, L. Xu, J. Ji, and X. Zhu, Design and analysis of a high torque density hybrid permanent magnet excited vernier machine, *Energies*, *15*(5), 2022, 1723.

[11] F. Xu, T. He, Z.Q. Zhu, Y. Wang, S. Cai, H. Bin, D. Wu, L. Gong, and J. Chen, Influence of slot number on electromagnetic performance of 2-pole high-speed permanent magnet motors with toroidal windings, *IEEE Transactions on Industry Applications*, *57*(6), 2021, 6023–6033.

[12] Z. Chen, N. Xing, H. Ma, Z. Li, J. Li, and C. Fan, Armature MMF and electromagnetic performance analysis of dual three-phase 10-pole/24-slot permanent magnet synchronous machine, *Archives of Electrical Engineering*, *72*(1), 2023, 189–210.

[13] P. Wang, W. Hua, G. Zhang, B. Wang, and M. Cheng, Principle of flux-switching permanent magnet machine by magnetic field modulation theory Part II: Electromagnetic torque generation, *IEEE Transactions on Industrial Electronics*, *69*(3), 2022, 2437–2446.

[14] P. Wang, W. Hua, G. Zhang, B. Wang, and M. Cheng, Principle of flux-switching permanent magnet machine by magnetic field modulation theory Part I: Back-electromotive-force generation, *IEEE Transactions on Industrial Electronics*, *69*(3), 2022, 2370–2379.

[15] Z. Zhu, Y. Huang, J. Dong, and F. Peng, Investigation study of the influence of pole numbers on torque density and flux-weakening ability of fractional slot concentrate winding wheel-hub machines, *IEEE Access*, 7, 2019, 84918–84928.

[16] C.C. Awah and O.I. Okoro, Analysis of torque ripple and total harmonic distortion of double-stator permanent magnet machine, *International Journal of Power and Energy Systems*, *38*(2), 2018, 69–76.

[17] Sh. Asgaria, R. Yazdanpanah, and M. Mirsalima, A dual-stator machine with diametrically magnetized PM: Analytical air-gap flux calculation, efficiency optimization, and comparison with conventional dual-stator machines, *Scientia Iranica D*, *29*(1), 208–216, 2022.

[18] J.T. Chen, Z.Q. Zhu, and D. Howe, Stator and rotor pole combinations for multi-tooth flux-switching permanent-magnet brushless AC machines, *IEEE Transactions on Magnetics*, *44*(12), 2008, 4659–4667.

[19] J.T. Chen and Z.Q. Zhu, Winding configurations and optimal stator and rotor pole combination of flux-switching PM brushless AC machines, *IEEE Transactions on Energy Conversion*, *25*(2), 2010, 293–302.

[20] C.C. Awah. Performance comparison of double stator permanent magnet machines, *Archives of Electrical Engineering*, *71*(4), 2022, 829–850.

[21] X. Liu, D. Wu, Z.Q. Zhu, A. Pride, R.P. Deodhar, and T. Sasaki, Efficiency improvement of switched flux PM memory machine over interior PM machine for EV/HEV applications, *IEEE Transactions on Magnetics*, *50*(11), 2014, 8202104.

[22] Z.Q. Zhu, Z.Z. Wu, D.J. Evans, and W.Q. Chu, A wound field switched flux machine with field and armature windings separately wound in double stators, *IEEE Transactions on Energy Conversion*, *30*(2), 2015, 772–783.

[23] W. Ullah, F. Khan, and S. Hussain, A comparative study of dual stator with novel dual rotor permanent magnet flux switching generator for counter rotating wind turbine applications, *IEEE Access*, 10, 2022, 8243–8261.

[24] J. Li, K. Wang, F. Li, S.S. Zhu, and C. Liu, Elimination of even-order harmonics and unipolar leakage flux in consequent-pole PM machines by employing N-S-Iron–S-N-Iron rotor, *IEEE Transactions on Industrial Electronics*, *66*(3), 2019, 1736–1747.

[25] X. Liu, W. Wang, S. Zhu, Y. Gao, and J. Fu, Design and optimization of a reverse salient pole flux controlled permanent magnet motor, *Progress In Electromagnetics Research C*, *129*(2), 2023, 127–141.

[26] Y. Gao, T. Kosaka, and R. Qu, Comparative study of high-current-density high-speed vernier permanent magnet machines for electric vehicle traction application, *Proc. of IEEE International Conf. on Electrical Machines (ICEM)*, Valencia, Spain, 2022, 1899–1905.

[27] W. Zhang, G.J. Li, Z.Q. Zhu, B. Ren, Y.C. Chong, and M. Michon, Demagnetization analysis of modular SPM machine based on coupled electromagnetic-thermal modelling, *Energies*, *16*(1), 2023, 131.

[28] C.C. Awah and Z.Q. Zhu, Influence of rotor pole number on electromagnetic performance of double-stator switched flux PM machines, *Proc. of the 13th IEEE Vehicle Power and Propulsion Conf. (VPPC2016)*, Zhejiang University, Hangzhou, China, 2016, 1–6.

[29] W. Hua, M. Cheng, Z.Q. Zhu, and D. Howe, Design of flux-switching permanent magnet machine considering the limitation of inverter and flux-weakening capability, *Proc. of IEEE Industry Applications Conf. Forty-First IAS Annual Meeting*, Tampa, USA, 2006, 2403–2410.

[30] A.A. Vahaj, A. Rahideh, and T. Lubin, General analytical magnetic model for partitioned-stator flux-reversal machines with four types of magnetization patterns, *IEEE Transactions on Magnetics*, *55*(11), 2019, 8107621.

[31] S.C. Wang, Y.C. Nien, and S.M. Huang, Multi-objective optimization design and analysis of V-shape permanent magnet synchronous motor, *Energies*, *15*(10), 2022, 3496.

[32] A.M. Ajamlooa, K. Abbaszadeha, and R. Nasiri-Zarandib, A novel transverse flux permanent magnet generator for small-scale direct drive wind turbine application: Design and analysis, *Scientia Iranica D*, *28*(6), 2021, 3363–3378.

Biographies

Chukwuemeka Chijioke AWAH was born in Nsukka, Nigeria. He received the B.Eng. and M.Eng. degrees in electrical engineering from the University of Nigeria, Nsukka in 2005 and 2009, respectively, and the Ph.D. degree in 2016 from the Department of Electronic and Electrical Engineering, the University of Sheffield, UK, under the Commonwealth Scholarship Award Scheme. He is a Senior Member of the Institute of Electrical and Electronics Engineers (SMIEEE), USA, and an active reviewer of many reputable journals: IEEE and other journals. He is also a member of the Nigerian Society of Engineers. He is registered with the Council for the Regulation of Engineering in Nigeria. He is a Faculty Member with the College of Engineering and Engineering Technology of Michael Okpara University of Agriculture, Umudike, Nigeria. He has published extensively in reputable local and international journals. His main research interests include modelling, design and analysis of electrical machines.